Intermetallic formation of Al-Fe and Al-Ni phases by ultrafast slurry aluminization (flash aluminizing)

Thomas Kepa, Fernando Pedraza, Fabien Rouillard

Version of Record: https://www.sciencedirect.com/science/article/pii/S0257897220306800
Manuscript_fdb226183bddbf2396afe42d705b0205

Intermetallic formation of Al-Fe and Al-Ni phases by ultrafast slurry aluminization (flash aluminizing)

Thomas Kepa[a,*], Fernando Pedraza[a,*], Fabien Rouillard[b]
[a]Laboratoire des Sciences de l'Ingénieur pour l'Environnement LaSIE UMR-CNRS 7356, Université de La Rochelle, Avenue Michel Crépeau, 17042 La Rochelle Cedex 1, France
[b]Den-Service de la Corrosion et du Comportement des Matériaux dans leur Environnement (SCCME), CEA, Université Paris-Saclay, F-91191 Gif-sur-Yvette, France
*Corresponding authors : thomas.kepa1@univ-lr.fr (T. Kepa), fpedraza@univ-lr.fr (F. Pedraza)

Abstract:

Aluminizing of Fe and Ni-based substrates is a conventional process often made by gas phase related techniques (CVD, pack cementation and above the pack), whereby the coating thickness is controlled by solid-state diffusion. Similar coatings can be achieved by slurry aluminizing where self-propagating high temperature synthesis and solid-state diffusion mechanisms are involved. The present work investigates ultrafast (5 min annealing) aluminization to reduce coating time and compares the results on pure iron and nickel substrates with a conventional slurry aluminizing treatment (2 and 5 h). The use of fast heating ramps (25 and 100°C/min) led to outwardly diffused coatings even with very high Al slurry activities. On nickel, the coatings were homogeneous while on iron, Kirkendall porosity occurred in the outermost layers due to the great dissolution of Fe in the Al melt and its subsequent outward diffusion towards to the Al source.

Keywords: Slurry aluminization ; iron aluminides ; nickel aluminides ; coatings

1. Introduction

Iron and nickel aluminide coatings are employed in different fields of application like power plants and aeronautical engines to improve the oxidation and corrosion of critical components due to their adequate properties [1, 2]. Many processes of aluminization like CVD [3, 4], pack cementation [5, 6], hot dipping [7, 8] and slurry [9, 10] are employed to obtain aluminide coatings. In CVD and pack cementation, aluminization occurs by gas adsorption followed by solid state diffusion [11]. The control of the aluminium activity in these processes enables to form high and low activity coatings [12]. The former grows by inward diffusion of aluminium at low temperatures (700 - 900°C) resulting in brittle Al-rich aluminide phases that requires subsequent annealing at higher temperatures. In low activity coatings, outward diffusion of iron or nickel is promoted at temperatures above 900°C, directly forming quasi-stoichiometric FeAl and NiAl phases. Pack cementation is cheaper than CVD but the processing times are relatively long in both processes. Hot-dipping is a much shorter (minutes) and cheaper process employed at industrial scale to produce aluminide coatings [13]. The substrate is immersed in molten aluminium for some seconds to a few minutes and the coating formed is generally Al-rich like in the high activity gas processes. Therefore, post diffusion heat treatment is necessary to obtain stoichiometric phases. Furthermore, this process is costly to maintain the aluminium bath molten and must be permanently protected against oxidation, so halide and chloride solid fluxes are sprayed on top of the bath [14].

Slurry aluminizing can be considered as an intermediate situation between CVD-like and hot-dip processes whereby the slurry containing Al microparticles is sprayed (or brushed) onto the substrate. Upon annealing, the coating is controlled by three main steps [15]: Al melts and wets the substrate, then the dissolution of the elements from the base material (i.e. Ni and/or Fe) brings about the self-propagating high temperature synthesis and finally once all the aluminium source is consumed, solid state diffusion takes place [15, 16]. The process usually involves a high activity of Al. Nevertheless, other experimental approaches have been investigated to reduce the Al activity by e.g., alloying Al with Cr [17] or by mixing Al and Cr particles or double layers [18] but the coating times are long (more than 6 hours). Recently, a first report on “fast aluminizing” has recently shown the possibility of

coating a Ni-rich iron alloy (Alloy 800H) in 3 to 5 min at temperatures between 700 and 1000°C in air by three different heating methods [19]. Although the coating method employed a very high activity (pure Al), the microstructures resembled the ones typically obtained from low activity processes. In addition, the coatings were relatively thin. However, the tests were performed in air and therefore, the Al microparticles in the slurry could have been oxidized leading to a lack of control of the formation of the coating. In addition, the precise heating (and cooling) ramps were not provided. Therefore, this paper investigates the formation of the aluminide coatings on pure Armco iron and on pure Ni for very short times (5 min) using a controlled fast heating ramp (100°C/min) in a thermogravimetric analyser (TGA). The results are compared with more conventional coating times (2 and 5 h) obtained at 25 and 100°C/min. All the coatings were obtained in argon to avoid the oxidation of the Al microparticles and two different slurry amounts were deposited to understand the effects of the Al supply on the coating mechanisms.

2. Experimental procedure

The pure (99.9%) nickel samples were 12.7 mm diameter discs with an approximate thickness of 2 mm. The pure (99.9%) Armco iron samples were cut from square bars of 1 cm^2 to obtain a thickness of 2 mm. The surfaces were ground with SiC P180 in order to obtain an adequate roughness onto which the slurry adheres to [5]. The samples were then rinsed with deionized water and then with ethanol in an ultrasonic bath for 3 minutes and finally dried in hot air.

The slurry was composed of a binder (57 wt.%) which is a mixture of polyvinyl alcohol (PVA) and water with a mass ratio 1:10 and microparticles of aluminum (43 wt.%) with an average size of 5-7 µm (Poudres Hermillon, 99.9% pure) [20]. A thick slurry deposit was sprayed with an airbrush on one side of the sample while the other side was covered with a thin deposit and then let to dry in ambient air. This approach aimed at studying the effects of deposited Al mass on the coating microstructure on the same sample. Two series of samples for each heat treatment were carried out for reproducibility purposes as shown in Table 1.

Table 1: Summary of heat treatments and amount of slurry deposited on the substrates.

		Amount of slurry deposited (mg.cm^{-2})	
Substrate	**Heat treatments at 1080°C**	**Thick deposit**	**Thin deposit**
Iron	5min (100°C/min)	9.0 ± 1.5	3.2 ± 0.5
	2h (25°C/min)		
	2h (100°C/min)		
	5h (100°C/min)		
Nickel	5 min (100°C/min)	10.5 ± 1	5.3 ± 1
	2h (25°C/min)		
	2h (100°C/min)		
	5h (100°C/min)		

Each coated sample was annealed in a thermobalance (SETARAM ATG 92) under Ar flow (20 mL.min^{-1}). The heating ramps were 100°C/min or25°C/min from room temperature to 1080°C. This temperature was chosen as it lies between the diffusion temperature typically used for the aluminization of ferritic-martensitic (1000°C) [21] and austenitic stainless steels (1100°C) [22] and for Ni-based superalloys (1100°C) [12]. The dwell times at 1080°C were set at 5 min (ultrafast aluminization), 2 and 5 h (conventional treatments). After annealing, the cooling rate was fixed at 50°C/min to maintain the microstructure, composition and phases that the coatings had at high temperature.

The crystal structure of the coatings was determined by X-Ray Diffraction (XRD) using a BRUKER AXS D8 Advance (Cu K_α radiation, λ= 0.15418 nm) in the θ-2θ mode between 10 and 90°. The coated samples were mounted in an epoxy resin to prepare the cross-sections, polished with diamond paste (1 µm) and etched. The aluminized iron samples were etched with a solution of 5 vol% Nital for 8 s. The coated nickel samples were etched with Kalling n°2 solution (5 g $CuCl_2$ + 100 mL HCl + 100 mL ethanol) for a few seconds.

The cross-sections before and after etching were observed under a LEICA DMRM optical microscope and a FEI Quanta 200F scanning-electron microscope (SEM). The chemical analyses were conducted with the EDAX detector coupled to the SEM.

3. Results

3.1 TGA curves during the heating ramps

Figure 1 shows the variation of specific mass (continuous lines) of both substrates in argon upon the fast heating ramps (dash lines). A similar variation was observed for both substrates and heating ramps. Each curve is composed of four domains like the ones reported by Rannou et al. [23]. The first domain corresponds to a mass gain due to the buoyancy of the TGA apparatus upon heating, which is followed by a strong mass loss between 250 and 400°C because of the evaporation of free water in the slurry. The third domain shows again a mass loss starting at 350°C that can be attributed to the decomposition of the binder [24]. Finally, the mass gain from 660°C onwards can be related to the melting of aluminium, which is immediately oxidized by the low oxygen content (2 vppm O_2 and 3 vppm H_2O) in the Ar bottle. The greatest mass losses in nickel can be associated with the greater deposited amounts of slurry (Table 1). Finally, the small mass loss around 770°C was only observed in the iron substrate and can be attributed to the ferromagnetic to paramagnetic transition in iron that modifies the electronic signal of the TGA. It can also be noticed that the slowest heating ramp (25°C/min) brings about an overall greater TGA mass than the fastest one (100°C/min), which can result from the enhanced hydroxylation and subsequent peripheral oxidation of the Al microparticles [15,24].

3.2 Fast aluminizing (5 min) on iron and nickel substrates

The SEM cross-sections of the coatings obtained on the Fe and Ni substrates at very fast heating rate (100°C/min) from room temperature to 1080°C and dwell time of 5 min are shown in Figure 2. Except for the thin coating on iron (Fig. 2b), all the coatings appear homogeneous and are more regular in thickness than the ones obtained by Bauer et al. at 1000°C for 3 minutes in air using three different heating methods (induction, heating mat, gas burner) [18]. On top of the coatings, the typical residues of the slurries [10] can also be observed.

Table 2: Main phases and average thicknesses of coatings obtained on iron from the thick and thin deposits.

		Thick deposit		Thin deposit	
Substrate	**Heat treatments at 1080°C**	**Phase formed**	**Thickness (µm)**	**Phase formed**	**Thickness (µm)**
Iron	5 min (100°C/min)	$FeAl_2$	20 ± 2	FeAl Fe(Al)	18 ± 2 30 ± 2
		FeAl	26 ± 2		
		Fe(Al)	35 ± 2		
	2h (25°C/min)	Fe(Al)	22 ± 2	Fe(Al)	10 ± 4
	2h (100°C/min)	FeAl	26 ± 2	Fe(Al)	9 ± 2
	5h (100°C/min)	Fe(Al)	19 ± 2	Fe(Al)	9 ± 2

The thinner deposits result in thinner aluminide coatings. Also, the aluminide coatings are thicker on iron than on nickel and the number of layers depend on the initial deposited amount of Al. Therefore, the thicker deposits result in three distinct layers on the iron substrate after 5 min at 1080°C (Table 2): $FeAl_2$ (20 µm), FeAl (26 µm) above and Fe(Al) (35 µm) below the porosity but only one layer (NiAl) around 50 µm thickness appears on nickel (Table 3), which agrees well with the findings of Mollard et al. [25] using a conventional heat treatment. In contrast, the thin deposits produce two-layered coatings in both substrates that are composed of FeAl (18 µm) above the porosity and Fe(Al) (30 µm) on the iron substrate while Al-rich (20 µm) and Al-poor (5 µm) β-NiAl layers grow in nickel according to the X-ray patterns and EDS profiles of Figs. 3 and 4, respectively. Kirkendall porosity only occurs in the iron aluminide coatings at the interface between the initial surface of the substrate and the slurry. This suggests that the intermetallic coatings are mainly formed by outward diffusion. Interestingly, the FeAl phase formed with just 25 at% Al instead of the Fe(Al) at 1080°C (Fig. 4 a), which can be explained because of the undefined border (dash line) between FeAl and Fe(Al) in the Al-Fe binary phase diagram [26]. In addition, the Ni_2Al_3 only detected by XRD in the coating grown from thick deposits on nickel is not observed by SEM/EDS and is therefore assumed to be located in slurry residues left over the diffusion coating.

Table 3: Main phases and average thicknesses of coatings obtained on nickel substrate from the thick and thin deposits.

		Thick deposit		Thin deposit	
Substrate	**Heat treatments at 1080°C**	**Phase formed**	**Thickness (µm)**	**Phase formed**	**Thickness (µm)**
Nickel	5 min (100°C/min)	NiAl (Al rich)	53 ± 3	NiAl (Al rich)	20 ± 2
				NiAl (Al poor)	5 ± 1
	2 h (25°C/min)	NiAl (Al rich)	28 ± 2	NiAl (Al poor)	25 ± 2
		NiAl (Al poor)	22 ± 2		
	2 h (100°C/min)	NiAl (Al rich)	25 ± 8	NiAl (Al poor)	30 ± 3
		NiAl (Al poor)	27 ± 1		
	5 h (100°C/min)	NiAl (Al rich)	15 ± 5	NiAl + Ni_3Al	22 ± 2
		NiAl (Al poor)	43 ± 2	Ni_3Al	8 ± 4

3.3 Conventional heat treatment time on pure iron

Figure 5 shows the optical micrographs of the cross sections of the iron samples coated with thick and thin deposits. The samples were heat-treated with 2 heating ramps (25 and 100°C/min) at 1080°C for 2 and 5 h under argon flow. All the coatings display Kirkendall porosity that is more marked than in the coatings obtained by fast aluminizing (5 min, 100°C/min). The pores seem also to grow with annealing time. In addition, the coatings have display columnar grains on top of which grows a thin layer whose thickness depends on the initial deposited amount of Al slurry and on the heat treatment. It can also be noted that the thickness of the top layer is relatively similar (19 vs. 26 µm) irrespective of the heat treatment (Table 2) when considering the standard deviation of the initial deposits (Table 1).

The X-ray patterns (Fig. 3) and the Al content retrieved by EDS (Fig. 4) clearly indicate that most of the coatings consist of a solid solution of Al into Fe , i.e. Fe(Al), except for the one grown at 100°C/min for 2h at 1080°C that displays an additional FeAl layer at the very top (Fig. 5b). Moreover, the depth of Al diffused in the iron substrate is twice than in nickel while its concentration decreases progressively towards the substrate except for the coating of Fig. 5b (100°C/min, 2h).

3.4 Conventional heat treatment time on pure nickel

The coatings formed on the nickel substrate for 2 and 5h of annealing are shown in Figure 6. The thick deposits of 10 mg/cm² (table 1) result in coating thicknesses in the range of 40-60 µm (Table 3), which is in good agreement with those obtained on pure nickel in other works at much slower heating rates

(5°C/min) and 700°C/2h + 1100°C/2h [27, 28]. These thick coatings display very large grains. Each grain has a bluish contrast at the top and a brown colour at the bottom. Like with the iron aluminides, the most significant difference between the thick coatings is the appearance of Kirkendall porosity in the coatings obtained at 100°C/min for 1080°C/2h (Fig. 4b). In contrast, the coatings grown from the thin deposits do not show either the top bluish contrast or the Kirkendall porosity. In addition, the final coating thickness obtained from the thin deposits is about half (25-30 µm) the one grown from the thick deposits, which indicates that the coating thickness depends on the initial amount of slurry deposited.

The X-ray patterns of the thick coatings clearly indicate the evolution from the Al-rich Ni_2Al_3 (5 min) to the NiAl phase (2 and 5 h) irrespective of the heating ramp. However, the fastest heating ramps (100°C/min) bring about the appearance of Ni_3Al already after 2h whose peaks intensity increases after 5h of annealing. This is not observed at 25°C/min. In the thin deposits, the NiAl phase obtained after 5 min is maintained after 1080°C/2h at 25°C/min but it markedly transforms into Ni_3Al at 100°C/min, in particular after 5h. The intermetallic phases found by XRD are in line with the EDS analyses of Fig. 4 for which the Al content shows that the NiAl phase is Al-rich at the coating/gas interface, hence explaining the bluish contrast. The composition profiles also demonstrate that the sharp coating/substrate interface obtained beyond 5 min of annealing is attenuated with increasing coating time to 2 and 5h. This results in a thin γ'-Ni_3Al layer grown between the main coating and the substrate. The tiny, Al_2O_3 peaks observed after 2 and 5h (100°C/min) correspond to a γ phase that Kolarik et al. also reported existing on the Al microparticles till 1100°C even though it is not the most thermodynamically stable phase [29].

4. Discussion

In order to determine the formation of coatings compared to the initial surface, half of the surface of the iron and nickel substrates was coated and heat treated at 1080°C for 2 hours with a fast heating ramp (100°C/min). The results are shown in figure 7. It appears that Kirkendall porosity occurs at the initial surface of the iron substrate (Fig. 7 (a)) and thus, the coating is mainly formed by outward

diffusion. In contrast, the coating is formed by both inward and outward diffusion in the nickel substrate (Fig. 7 (b)).

A schematic evolution of the coatings obtained on pure iron from room temperature until 1080°C with a fast heating ramp (100°C/min) is shown in Figure 8. At room temperature (step 1), the grain size of the substrate is small (around 30 µm). Upon heating to intermediate temperatures (about 700°C), the size of the grains remains basically the same (Fig.8, step 2). At the temperature of 700°C, a main endotherm was detected by DSC (not shown) and can be associated with the melting of Al. This indicates that the melting of Al under standard conditions (660°C) is delayed because of the fast heating ramp. Therefore, the overheated Al suddenly melts and dissolves Fe. The reaction between Al and Fe brings about the formation of Fe_2Al_5 following the c-direction of the faulty orthorhombic structure that results in the typical tongue-like morphology. Takata et al. supports that this mechanism is further enhanced by the flow of vacancies under local stress fields [30]. Similar coating microstructures have been also reported by Kobayashi et al. when carbon steel was hot dipped at 850°C and 900°C for 300 s of immersion [31].

The dissolution of iron in the aluminium melt between 700 and 1080°C and upon the 5 min of reaction (Fig.8, step 3), provokes the onset of formation of the pores at the melt/substrate interface (Fig. 7 (a)). The same kind of porosity is often observed on steel substrates aluminized by CVD [4], hot-dipping [14, 32] and slurry [33] due to the higher Fe outward diffusion rate, which is unbalanced by the inward diffusion of Al. Such interfacial porosity separates two main sublayers. The top sublayer grows towards the slurry reservoir resulting in an Al gradient of intermetallic compounds ($FeAl_2$ over FeAl). In contrast, the bottom coating sublayer is composed of the solid solution Fe(Al) and display columnar morphology. This is in line with the works of Murakami et al. [34], who obtained the same morphology of Fe(Al) grains on pure iron. They explained that the columnar grains of Fe(Al) are produced by the first intermetallic phase formed upon the hot dipping process (i.e. Fe_2Al_5), which displays a tongue-like morphology. Then, Al diffuses through Fe_2Al_5 and the grains of the α-Fe substrate grow by enhanced incorporation of Al supplied from the previously nucleated the Fe_2Al_5 columnar grains. The formation of the coating occurs so rapidly that the concentration of Al reaches about 3 at% at 80 µm deeper from the coating/substrate interface after 5 min at 1080°C (Fig. 4(a)).

Extending the aluminizing time to 2 and 5 hours (Fig.8, steps 4 and 5) brings about a drastic decrease of the Al content in the coating as it diffuses further into the substrate (140 and 190 µm for respectively, 2 and 5 h). In addition, the Kirkendall porosity increases with increasing time. Furthermore, the size of the tongue-like grains of the coating below porosity increases by diffusion of Al into the α-Fe. Simultaneously, the grain size at the core of the substrate increased from about 30 µm of the as-received samples and samples heat treated at 700°C (not shown) to about 55 µm after coating at 1080°C (5 min, 2 and 5 h). Since no Al reached the core of the iron substrate, other growth mechanisms shall occur. Antonione et al. [35] reported that the growth rate of the grains in iron was particularly fast with increasing temperature though dependant on the amount of impurities that could block the growth after the release of stresses and dislocation glide. Such grain growth derives from the self-diffusion coefficients of iron in bcc (α-Fe) that also increase with temperature according to Mehrer et al. [36]. In the particular case of unstrained Armco iron, the exponential grain growth was triggered from 850°C due to the minor impurities while on the strained material the onset temperature was lower and depended on the level of deformation. Over a given temperature, the grain growth is inhibited by polygonization [35]. However, we did not stop the tests to observe the onset temperature at which the grains grew drastically but at 1080°C they did not grow anymore at either 5 min, 2 and 5h. This implies that the flux of Fe towards the coating is constant at 1080°C. The outward diffusion of Fe is thus ruled by the concentration gradient between the core and the Al rich top layers of the coating and by the derived vacancies created by the dissolution of Al in the α-Fe(Al) that increases further the diffusion coefficient of iron [36]. As a result, the Al content at the surface decreases with increasing the dwell time as demonstrated in the Al composition profiles of the thick deposits (Fig 4 (a)).

Figure 9 shows schematically the evolution of the coating on the nickel substrate. As opposed to the iron substrate, the grain size at the core of the substrate (Fig. 9, step 1) is not affected by the heat treatment (average size of 500 µm). For the flash aluminizing for 5 min at 1080°C (Fig. 9, step 2), coarse-grains of Al-rich NiAl coating form equally above and below the initial substrate surface (Fig. 7 (b)). Then, with increasing coating time, the outward diffusion of nickel is promoted, which

consequently decreases the aluminium content (Fig. 9, step 3). After 5 hours of annealing (Fig. 9, step 4), the initial Al-rich NiAl fully transforms into Al-poor NiAl, yet with a columnar grain morphology.

Overall, the fast heating rates employed in this study (25 and 100°C/min) involve a flash aluminization of the substrates by self-propagating high temperature synthesis in agreement with other works. For instance, Biswas et al. [37] reported that the combustion temperature was affected by the heating rate (up to 60°C/min in their studies) when making Al microparticles (42 µm) react with Ni microparticles (110 µm). The combustion temperature increases when the heating ramps increase too (e.g. 1150°C, 1400°C and 1800°C for respectively 10, 25 and 50°C/min). Moreover, the combustion temperature could reach 1800°C by heating at 25°C/min the smallest Ni particles (11 µm) [37]. A heating rate of 15°C/min also shifted the ignition temperature from 640 to 675°C [37]. We have also observed such shift in our work but our faster rates (25 and 100°C/min) shifted the Al melting to 700°C and then combustion can occur and probably reach even higher temperatures. For instance, Zhu et al. [38] reported temperatures about 1875°C when making molten Al (660°C) react with Ni under adiabatic conditions, i.e. with no heat exchange.

5. Conclusions

Slurry aluminide coatings were fabricated on pure iron and nickel substrates using fast heating ramps (25 and 100°C/min). It was demonstrated that a very short heat treatment at 1080°C for 5 minutes (heating ramp: 100°C/min and cooling rate: 50°C/min) is sufficient to obtain homogeneous coatings on both substrates. An Al-rich β-NiAl was formed on nickel from both the thick and the thin slurry deposits. In contrast, dual-layered coatings (top $FeAl_2$ and bottom B2-FeAl) grew on iron from the thick deposit while the B2-FeAl phase was solely obtained from the thin slurry deposit. The Kirkendall pores generated at the initial surface of the iron substrate expanded with increasing coating time (2h and 5h) at 1080°C. Decreasing the heating ramp to 25°C/min does not seem to have any influence on the nickel aluminides while it decreased the porosity in the coatings on iron. In addition, the two-fold increase of the initial slurry thickness (5 mg/cm² to 10 mg/cm²) resulted in twice the thickness of the aluminide coatings on nickel (20-30 µm to 40-60 µm).

Overall, the flash aluminizing method of iron and nickel substrates results in microstructures, compositions and crystal phases very alike to the ones obtained using conventional gas aluminizing processes (CVD-like) but in much shorter times (5 min) similar to those of hot dipping. In contrast to the latter, it appears that the slurry could be sprayed on site without size limitation as in hot dipping. Further studies are currently ongoing to assess the influence of alloying elements in the formation of aluminide coatings on real alloys by flash aluminizing.

Authors' contributions

F. Pedraza has designed the study. The first and second authors have contributed to the acquisition of data and have participated in drafting the article or revising it critically for important intellectual content. The three authors have made substantial contributions the analysis and interpretation of data. Finally, all authors give final approval of the submitted version.

Acknowledgements

The authors gratefully acknowledge to the French Alternative Energies and Atomic Energy Commission (CEA) for the partial funding of this research and acknowledge Prof. Bonnet for fruitful discussions.

References

[1] P. C Patnaik, Intermetallic coatings for high temperature applications: A review, Mater. Manuf. Process. 04 (1989) 133-152.

[2] J. R. Nicholls, Designing oxidation-resistant coatings, JOM. 52 (2000) 28-35.

[3] F. Pedraza, C. Gomez, M.C. Carpintero, M.P. Hierro, F.J. Pérez, On the aluminisation of stainless steel by CVD in fluidised beds, Surf. Coat. Technol. 190 (2005) 223-230.

[4] Y. Zhang, B. A. Pint, K. M. Cooley, J. A. Haynes, Formation of aluminide coatings on Fe-based alloys by chemical vapor deposition, Surf. Coat. Technol. 202 (2008) 3839-3849.

[5] L. Levin, A. Ginzburg, L. Klinger, T. Werber, A. Katsman, P. Schaaf, Controlled formation of surface layers by pack aluminization, Surf. Coat. Technol. 106 (1998) 209-213.

[6] Z. D. Xiang, J. S. Burnell-Gray, P. K. Datta, Aluminide coating formation on nickel-base superalloys by pack cementation process, J. Mater. Sci. 36 (2001) 5673-5682.

[7] H. Glasbrenner, O. Wedemeyer, Comparison of hot dip aluminised F82H-mod steel after different subsequent heat treatments, J. Nucl. Mater. 257 (1998) 274-281.

[8] C.-J. Wang, S.-M. Chen, Microstructure and cyclic oxidation behavior of hot dip aluminized coating on Ni-base superalloy Inconel 718, Surf. Coat. Technol. 201 (2006) 3862-3866.

[9] A. Agüero, J.C. del Hoyo, J. García de Blas, M. García, M. Gutiérrez, L. Madueño, S. Ulargui, Aluminum slurry coatings to replace cadmium for aeronautic applications, Surf. Coat. Technol. 213 (2012) 229-238.

[10] F. Pedraza, C. Boulesteix, M. Proy, I. Lasanta, T. de Miguel, A. Illana, F.J. Pérez, Behavior of Slurry Aluminized Austenitic Stainless Steels under Steam at 650 and 700 °C, Oxid. Met. 87 (2017) 443-454.

[11] F. Bozza, G. Bolelli, C. Giolli, A. Giorgetti, L. Lusvarghi, P. Sassatelli, A. Scrivani, A. Candeli, M. Thoma, Diffusion mechanisms and microstructure development in pack aluminizing of Ni-based alloys, Surf. Coat. Technol. 239 (2014) 147-159.

[12] G. W. Goward, D. H. Boone, Mechanisms of formation of diffusion aluminide coatings on nickel-base superalloys, Oxid. Met. 3 (1971) 475-495.

[13] H. Silman, Continuous Hot-Dip Aluminizing of Steel Strip, Trans. IMF. 40 (1963) 85-92.

[14] M. Abro, D. Lee, Effect of Al Hot-Dipping on High-Temperature Corrosion of Carbon Steel in N2/0.1% H2S Gas, Metals. 6 (2016) 38-43.

[15] M. C. Galetz, X. Montero, M. Mollard, M. Günthner, F. Pedraza, M. Schütze, The role of combustion synthesis in the formation of slurry aluminization, Intermetallics. 44 (2014) 8-17.

[16] B. Bouchaud, B. Rannou, F. Pedraza, Slurry aluminizing mechanisms of Ni-based superalloys incorporating an electrosynthesized ceria diffusion barrier, Mater. Chem. Phys. 143 (2013) 416-424.

[17] X. Montero, M. C. Galetz, M. Schütze, Low-activity aluminide coatings for superalloys using a slurry process free of halide activators and chromates, Surf. Coat. Technol. 222 (2013) 9-14.

[18] B. Grégoire, G. Bonnet, F. Pedraza, Development of a new slurry coating design for the surface protection of gas turbine components, Surf. Coat. Technol. 374 (2019) 521-530.

[19] J. T. Bauer, X. Montero, M. C. Galetz, Fast heat treatment methods for al slurry diffusion coatings on alloy 800 prepared in air, Surf. Coat. Technol. 381 (2020) 125140.

[20] M. Mollard, Elaboration de systèmes barrière thermique par barbotine : comportement du nickel et de ses superalliages revêtus en oxydation cyclique à haute température, PhD Thesis, Université de La Rochelle.

[21] C. Boulesteix, F. Pedraza, M. Proy, I. Lasanta, T. de Miguel, A. Illana, F.J. Pérez, Steam Oxidation Resistance of Slurry Aluminum and Aluminum/Silicon Coatings on Steel for Ultrasupercritical Steam Turbines, Oxid. Met. 87 (2017) 469-479.

[22] C. Boulesteix, B. Grégoire, F. Pedraza, Oxidation performance of repaired aluminide coatings on austenitic steel substrates, Surf. Coat. Technol. 326 (2017) 224-237.

[23] B. Rannou, Slurry coatings from aluminium microparticles on Ni-based superalloys for high temperature oxidation protection, PhD Thesis, Université de La Rochelle.

[24] B. Rannou, F. Velasco, S. Guzmán, V. Kolarik, F. Pedraza, Aging and thermal behavior of a PVA/Al microspheres slurry for aluminizing purposes, Mater. Chem. Phys. 134 (2012) 360-365.

[25] M. Mollard, B. Rannou, B. Bouchaud, J. Balmain, G. Bonnet, F. Pedraza, Comparative degradation of nickel aluminized by slurry and by pack cementation under isothermal conditions, Corros. Sci. 66 (2013) 118-124.

[26] Akshansh Mishra, Friction stir welding of dissimilar metal: A Review, I.J.R.A.S.E.T. 6 (2018).1551-1559

[27] F. Pedraza, M. Mollard, B. Rannou, J. Balmain, B. Bouchaud, G. Bonnet, Potential thermal barrier coating systems from Al microparticles. Mechanisms of coating formation on pure nickel, Mater. Chem. Phys. 134 (2012) 700-705.

[28] F. Pedraza, M. Proy, C. Boulesteix, P. Krukovskyi, M. Metel, Slurry aluminizing of IN-800HT austenitic stainless steel and pure nickel. Correlations between experimental results and modelling of diffusion: Slurry aluminizing of IN-800HT, Mater. Corros. 67 (2016) 1059-1067.

[29] V. Kolarik, M. del M. Juez-Lorenzo, H. Fietzek, Oxidation of Micro-Sized Spherical Aluminium Particles, Mater. Sci. Forum. 696 (2011) 290-295.

[30] N. Takata, M. Nishimoto, S. Kobayashi, M. Takeyama, Crystallography of Fe2Al5 phase at the interface between solid Fe and liquid Al, Intermetallics. 67 (2015) 1-11.

[31] S. Kobayashi, T. Yakou, Control of intermetallic compound layers at interface between steel and aluminum by diffusion-treatment, Mater. Sci. Eng. A. 338 (2002) 44-53.

[32] J. Chen, G. Z. Dai, J. W. Zhao, X. M. Huang, J. Han, Optimization of Process Parameters of Hot-Dip Aluminized Coating, Adv. Mater. Res. 391-392 (2011) 46-50.

[33] A. Agüero, V. González, M. Gutiérrez, Long Term Diffusion Studies in Fe Aluminide Coatings Deposited by Slurry Application on Ferritic Steel, Defect Diffus. Forum. 289-292 (2009) 243-251.

[34] K. Murakami, N. Nishida, K. Osamura, Y. Tomota, T. Suzuki, Aluminization of high purity iron and stainless steel by powder liquid coating, Acta Materialia, 52 (2004) 2173-2184.

[35] C. Antonione, G. Della Gatta, G. Riontino, G. Venturello, Grain growth and secondary recrystallization in iron, Jour. Mater. Sci. 8 (1973) 1-10.

[36] H. Mehrer, M. Luckabauer, W. Sprengel, Self- and Solute Diffusion, Interdiffusion and Thermal Vacancies in the System Iron-Aluminium, Defect Diffus. Forum. 333 (2013) 1-25.

[37] A. Biswas, S. K. Roy, K. R. Gurumurthy, N. Prabhu, S. Banerjee, A study of self-propagating high-temperature synthesis of NiAl in thermal explosion mode, Acta Materialia, 50 (2002) 757-773.

[38] P. Zhu, J. C. M. Li, C. T. Liu, Adiabatic temperature of combustion synthesis of Al-Ni systems, Mater. Sci. Eng. A. 357 (2003) 548-257.

List of figure captions

Figure 1: TGA curves (straight lines) obtained upon aluminization of (a) iron and (b) nickel substrates during the heating ramps (dash lines)

Figure 2: SEM cross-sections (BSE) of (a, b) iron and (c, d) nickel samples aluminized for 5 min at 1080°C and a fast heating ramp (100°C/min) for thin and thick deposits.

Figure 3: XRD patterns after the different coating treatments on the (a, b) iron and (c, d) nickel substrates from the thin and thick slurry deposits.

Figure 4: EDS composition profiles of the coatings obtained on the (a) iron and (b) nickel substrates from the thin and thick slurry deposits.

Figure 5: Optical cross-sections of the coatings grown on the iron substrate from the (a, b, c) thick and (d, e, f) thin deposits using different times at 1080°C and different heating ramps.

Figure 6: Optical of cross-sections of the coatings grown on the nickel substrate from the (a, b, c) thick and (d, e, f) thin deposits using different times at 1080°C and different heating ramps.

Figure 7: Iron (a) and nickel (b) substrates half-coated at 1080°C/2h (100°C/min). The red dash line indicates the initial surface of the substrate.

Figure 8: Schematic mechanism of coating formation on iron substrate from thick deposits with a fast heating ramp (100°C/min).

Figure 9: Schematic mechanism of coating formation on nickel substrate from thick deposits with a fast heating ramp (100°C/min).

Figures

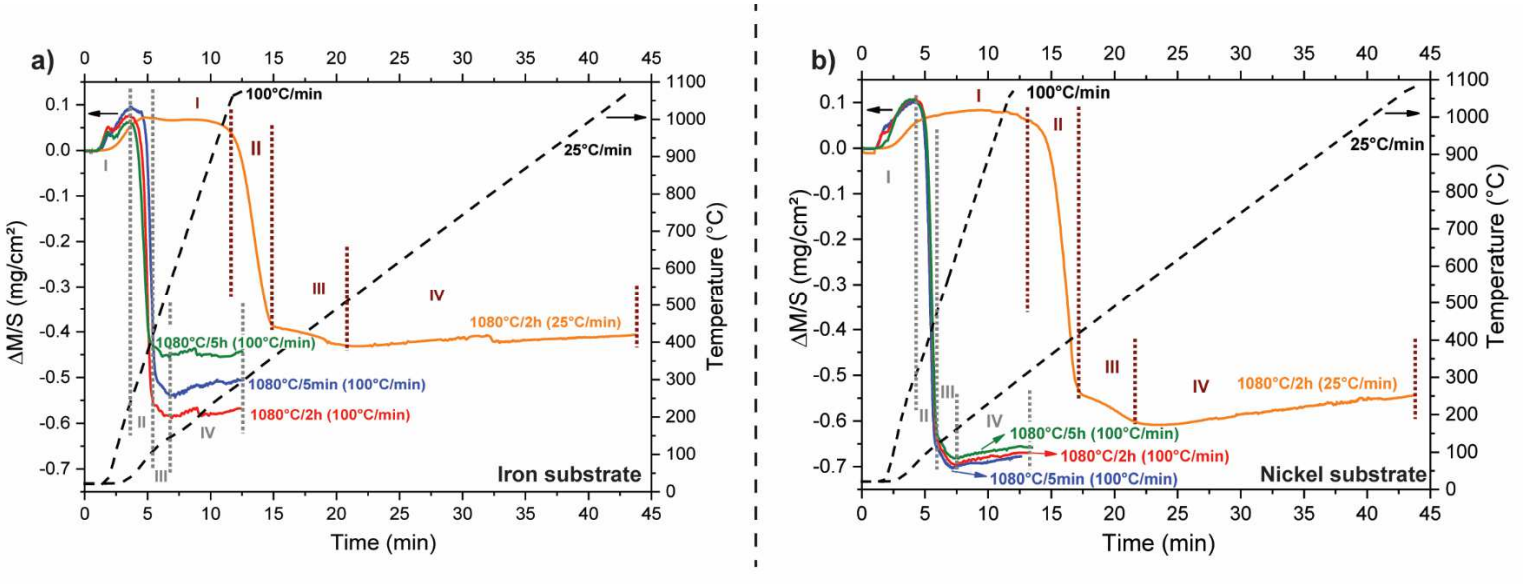

Fig. 1

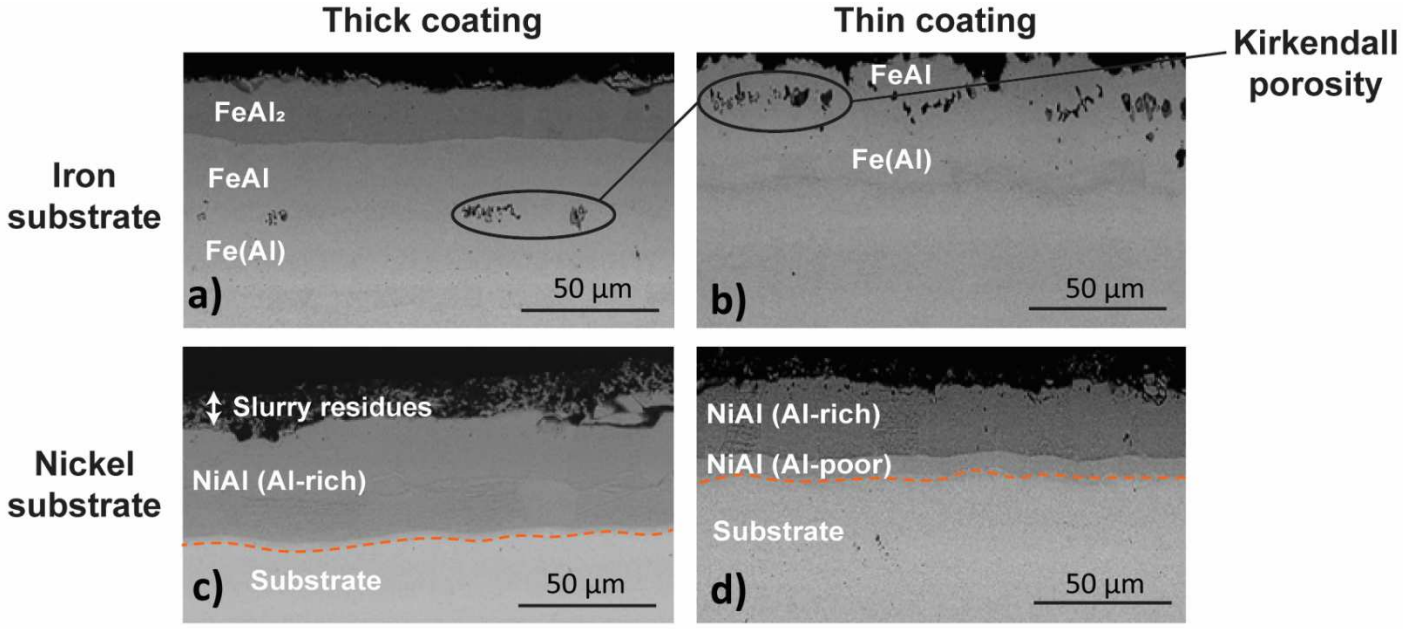

Fig. 2

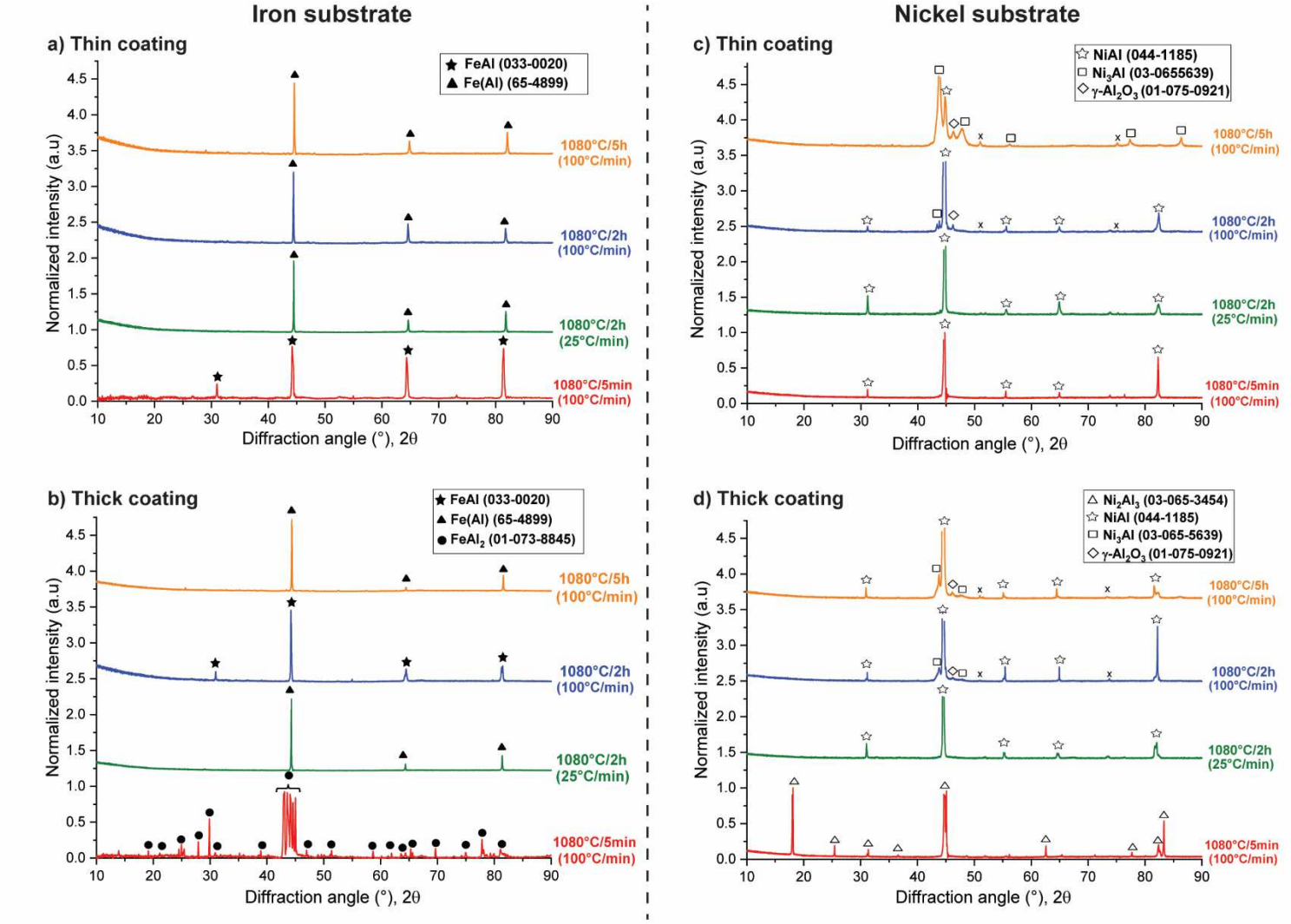
Iron substrate
Nickel substrate
a) Thin coating
b) Thick coating
c) Thin coating
d) Thick coating
FeAl (033-0020)
Fe(Al) (65-4899)
FeAl2 (01-073-8845)
NiAl (044-1185)
Ni3Al (03-0655639)
γ-Al2O3 (01-075-0921)
Ni2Al3 (03-065-3454)
Ni3Al (03-065-5639)
1080°C/5h (100°C/min)
1080°C/2h (100°C/min)
1080°C/2h (25°C/min)
1080°C/5min (100°C/min)
Normalized intensity (a.u)
Diffraction angle (°), 2θ

Fig. 3

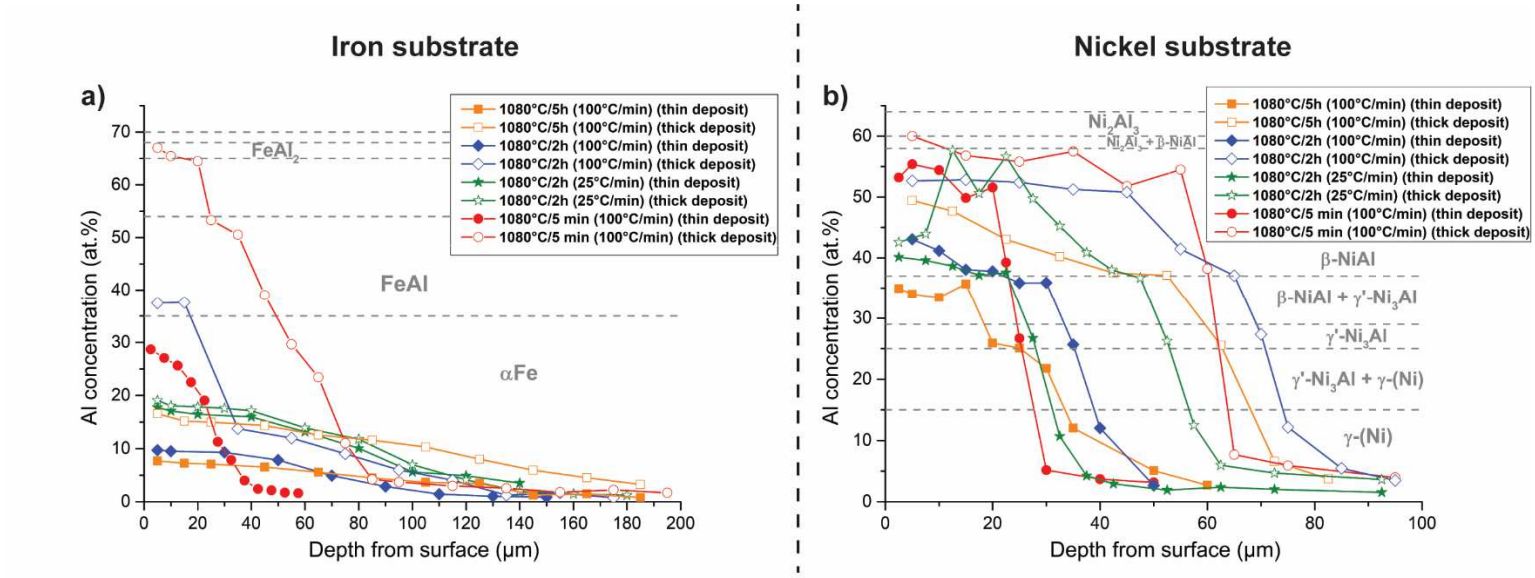
Iron substrate
Nickel substrate
a)
b)
Al concentration (at.%)
Depth from surface (μm)
FeAl2
FeAl
αFe
Ni2Al3
Ni2Al3 + β-NiAl
β-NiAl
β-NiAl + γ'-Ni3Al
γ'-Ni3Al
γ'-Ni3Al + γ-(Ni)
γ-(Ni)
1080°C/5h (100°C/min) (thin deposit)
1080°C/5h (100°C/min) (thick deposit)
1080°C/2h (100°C/min) (thin deposit)
1080°C/2h (100°C/min) (thick deposit)
1080°C/2h (25°C/min) (thin deposit)
1080°C/2h (25°C/min) (thick deposit)
1080°C/5 min (100°C/min) (thin deposit)
1080°C/5 min (100°C/min) (thick deposit)

Fig. 4

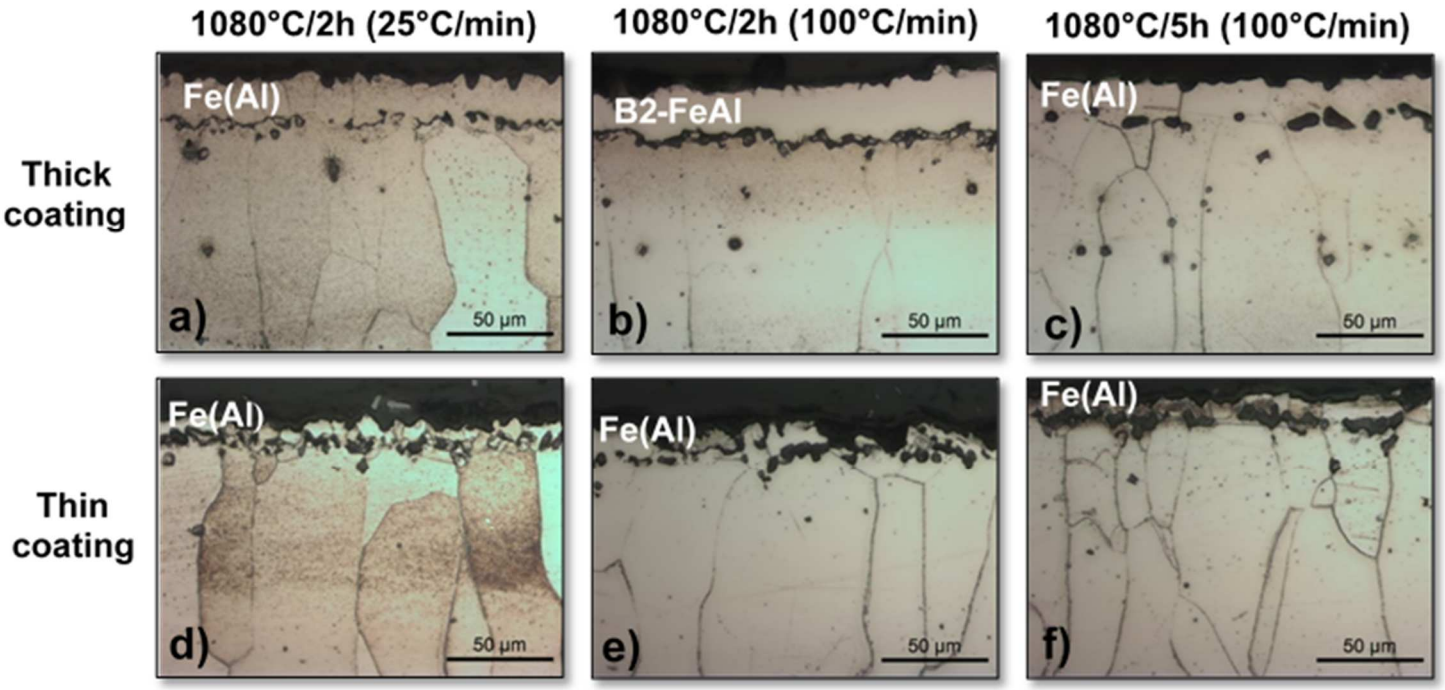
1080°C/2h (25°C/min)
1080°C/2h (100°C/min)
1080°C/5h (100°C/min)
Thick coating
Thin coating
Fe(Al)
B2-FeAl
a)
b)
c)
d)
e)
f)
50 μm

Fig. 5

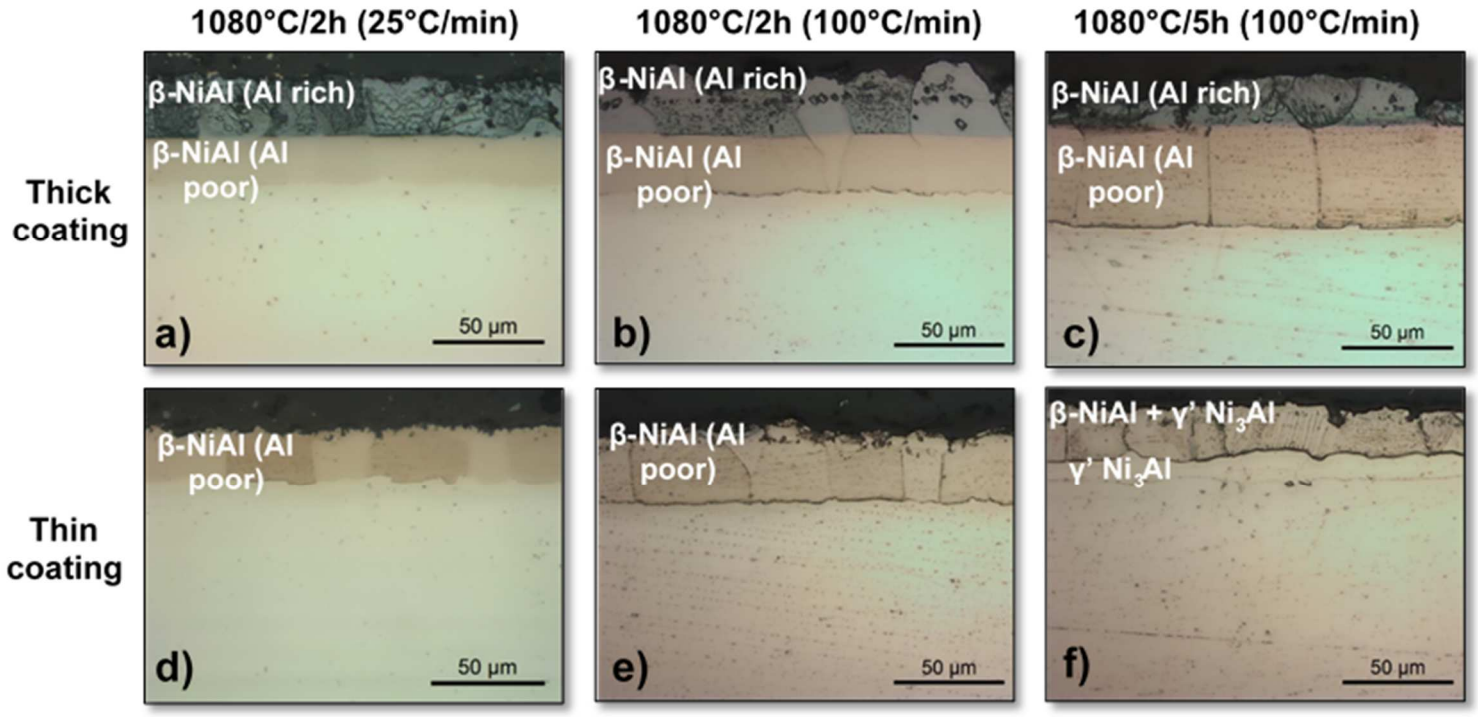
1080°C/2h (25°C/min)
1080°C/2h (100°C/min)
1080°C/5h (100°C/min)
Thick coating
Thin coating
β-NiAl (Al rich)
β-NiAl (Al poor)
β-NiAl + γ' Ni3Al
γ' Ni3Al
50 µm
a)
b)
c)
d)
e)
f)

Fig. 6

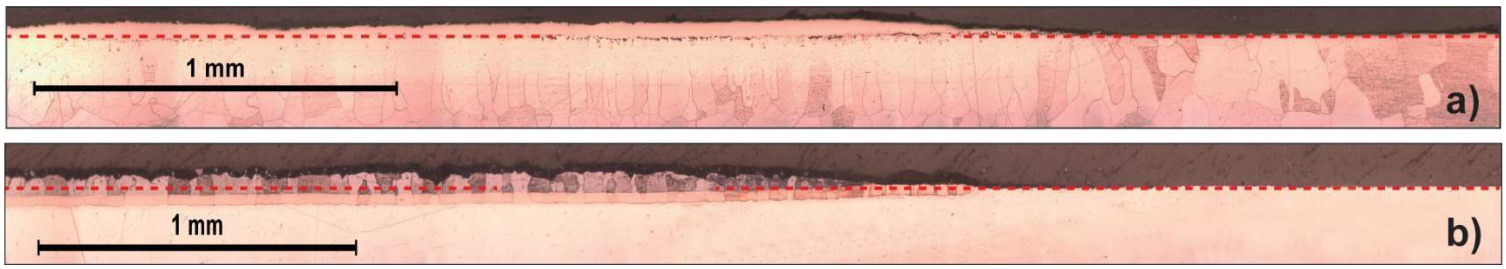
1 mm
a)
1 mm
b)

Fig. 7

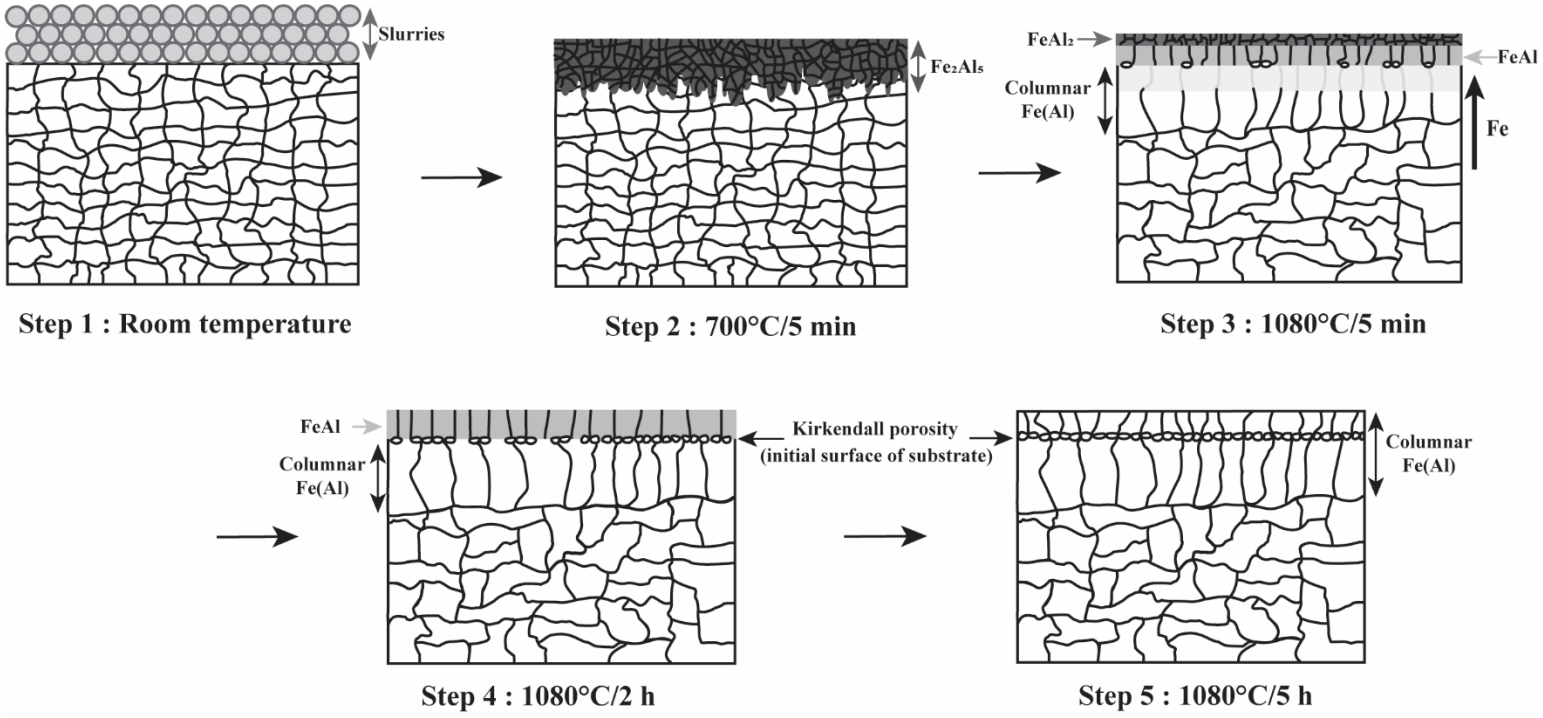
Slurries
Step 1 : Room temperature
Fe2Al5
Step 2 : 700°C/5 min
FeAl2
FeAl
Columnar
Fe(Al)
Fe
Step 3 : 1080°C/5 min
FeAl
Columnar
Fe(Al)
Kirkendall porosity
(initial surface of substrate)
Columnar
Fe(Al)
Step 4 : 1080°C/2 h
Step 5 : 1080°C/5 h

Fig. 8

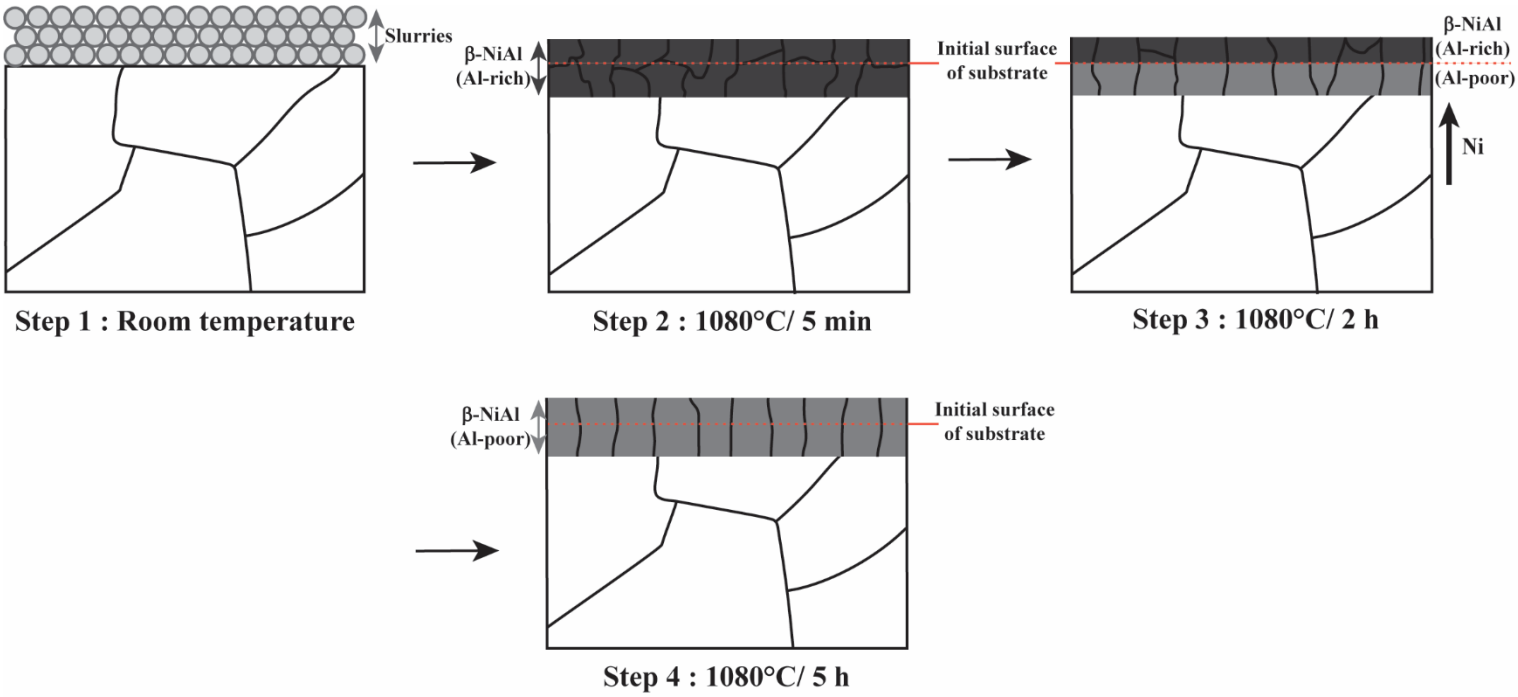
Slurries
Step 1 : Room temperature
β-NiAl
(Al-rich)
Initial surface
of substrate
Step 2 : 1080°C/ 5 min
β-NiAl
(Al-rich)
(Al-poor)
Ni
Step 3 : 1080°C/ 2 h
β-NiAl
(Al-poor)
Initial surface
of substrate
Step 4 : 1080°C/ 5 h

Fig. 9